Journal of Coordination Chemistry

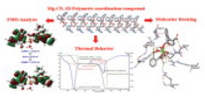

ISSN: 0095-8972 (Print) 1029-0389 (Online) Journal homepage: www.tandfonline.com/journals/gcoo20

Systematic investigation of coordination compounds in the CuCl–DABCO–HCl composition space diagram

Andrii Hultiaiev & Evgeny Goreshnik

To cite this article: Andrii Hultiaiev & Evgeny Goreshnik (03 Jul 2026): Systematic investigation of coordination compounds in the CuCl–DABCO–HCl composition space diagram, Journal of Coordination Chemistry, DOI: 10.1080/00958972.2026.2694413

To link to this article: https://doi.org/10.1080/00958972.2026.2694413

JOURNAL OF COORDINATION CHEMISTRY
https://doi.org/10.1080/00958972.2026.2694413

Systematic investigation of coordination compounds in the CuCl–DABCO–HCl composition space diagram

Andrii Hultiaiev and Evgeny Goreshnik

Department of Inorganic Chemistry and Technology, Jožef Stefan Institute, Ljubljana, Slovenia

ABSTRACT

This study is devoted to the investigation of the copper (I) chloride–HCl – 1,4-diazabycyclo[2.2.2]octane composition diagram. Electrochemical and solvothermal syntheses were performed in this investigation. $CuCl_2$, which is more soluble than CuCl, compropportionates with copper anode in the electrochemical technique and with copper powder in the solvothermal method, forming monovalent copper Cu^I *in situ*. HCl promotes the formation of different protonated forms of diamine by forming a specific pH of the reaction mixtures. The **$(HDABCO^+)Cu_2Cl_3$** compound was synthesized in ethanol by electrochemical and solvothermal techniques. The **$Cu_2Cl_2(DABCO)$** compound was synthesized electrochemically in ethanol and in methanol. The compound **$[Cu_4Cl_6(DABCO)][Cu(H_2O)_4]$** was synthesized under solvothermal conditions in ethanol at 150 °C. Decreasing the temperature to 130 °C leads to the formation of compound **$Cu_4Cl_7(HDABCO^+)_3$**. Changing the solvent to methanol using the same amounts of reagents leads to the **$(HDABCO^+)Cu_5Cl_6(DABCO)$** formation. CuCl reacts under solvothermal conditions with an ethanol solution of DABCO, forming **$Cu_6Cl_6(DABCO)_2$**. Formed *in situ* by the decomposition of acetonitrile under hard solvothermal conditions (170 °C), CN groups play a key role in the formation of the compound **$(HDABCO^+)CuCl(CN)$.**

ARTICLE HISTORY
Received 15 October 2025
Accepted 13 June 2026

KEYWORDS
Electrochemical synthesis; copper chloride; DABCO ligand; polynuclear copper complexes; composition space diagram

CONTACT Andrii Hultiaiev andrii.hultiaiev@ijs.si Department of Inorganic Chemistry and Technology, Jožef Stefan Institute, Ljubljana, 1000, Slovenia.

Supplemental data for this article can be accessed online at https://doi.org/10.1080/00958972.2026.2694413.

GRAPHICAL ABSTRACT

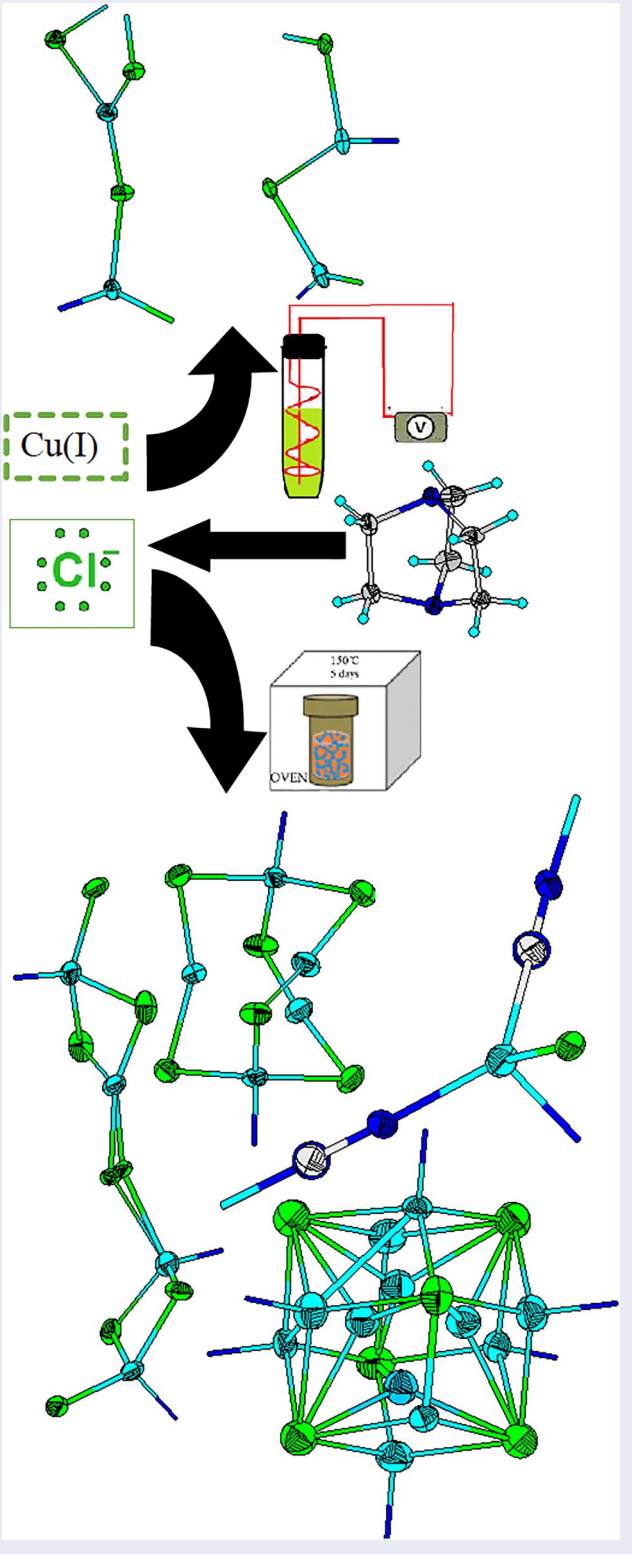

1. Introduction

Among coordination chemists, there is a rapidly growing interest in polynuclear metal complexes based on copper (PNCCs), which is caused by the growing interest in their properties, such as structural flexibility, tunable coordination behavior, redox activity, magnetic properties, strong luminescence, structural tunability, and a widespread functional range [1]. That is why they are actively used for catalysis in organic synthesis, photoactive elements (OLEDs), components for gas adsorption and separation, and biomedical applications (because of antioxidant, antimicrobial, anticancer, and anti-inflammatory properties). This arises from the awareness that pairs or clusters of metal ions appear to mediate certain chemical reactions differently from complexes of isolated metal centers [2]. In the case of monovalent copper Cu^{I} as a metal center, its d^{10} electronic configuration and tendency for low coordination numbers ($\leq$ 4) lead to a highly dynamic coordination sphere and strong cuprophilic interactions [3]. These features are vital to the fascinating photophysical and catalytic properties of Cu(I) clusters. Cu^{I}-based PNCs favor tetrahedral arrangements controlled by steric factors rather than ligand field effects. However, 4-coordinate (square-planar) Cu(I)-based coordination compounds also occur, especially in systems with very bulky ligands or a low coordination number [4,5]. It has already been discovered that the copper(I) chloride-based compounds can form a wide range of inorganic fragment shapes: from discrete dimers [6], bicyclic trimers [7], prismane-like hexamers [8], cubane [9,10] types, up to the infinite 1-D chains [11], 2-D layers [12], and 2-D and 3D nets [13]. Also, some of them have a 3-D porous structure [14]—metal-organic frameworks. The formation of zeolite-like metal-organic frameworks (ZMOFs) also requires a metal coordination center with a preferred tetrahedral geometry, angular ditopic N-donor organic ligands [15] as linkers, and anions to ensure charge balance. In this context, monovalent copper with its electronic configuration attracts attention as a metal center suitable for the MOF′s construction of various geometric structures.

In nature, many metal-N-donor coordination compounds seem to have active sites comprising pairs of metal ions [16] nearby. Such a candidate for an organic N-donor ditopic ligand could be alicyclic nitrogen-based linker DABCO (1,4- diazabycyclo [2] octane, tryethylenediamine).

This work is devoted to the systematic study of Cu^{I}-Cl-DABCO-containing coordination compounds formation using a systematic approach with a CuCl-DABCO-HCl composition space diagram. This approach has proven to be effective in the studies of other systems, giving a large structural diversity of coordination compounds there [17]. The CSD CCDC global search shows that some compounds in this system have been discovered earlier (Figure 1). However, it covers a narrow range of the molar ratios of reagents with a high concentration of hydrochloric acid [11,14, 18–20] on the diagram. The CCDC contains only six compounds [19] with monovalent copper ions and diprotonated H_2DABCO^{2+} cations, four compounds with monoprotonated $HDABCO^{+}$ cations coordinated with monovalent copper by the unprotonated N-atom, and two compounds with unprotonated DABCO ligands coordinated with monovalent copper ions by both N-atoms. Also, the critical factor is that even a minor change of

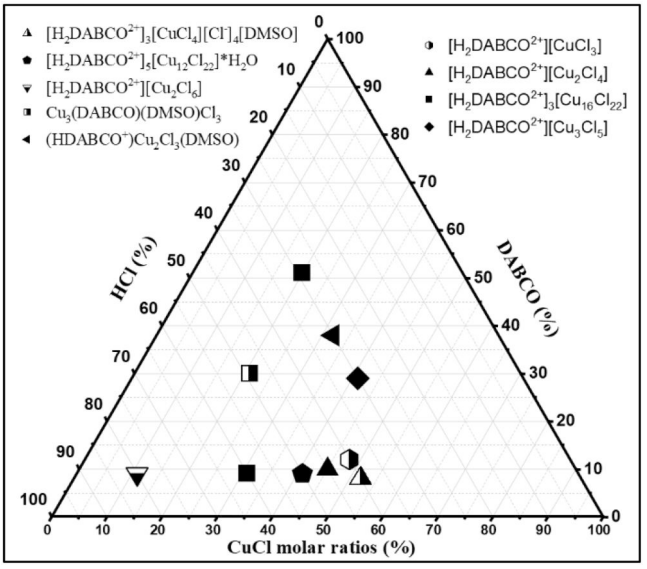

Figure 1. Previously discovered Cu-Cl-DABCO-containing coordination compounds from CCDC.

the synthetic conditions, which includes temperature, solvent, pH, concentrations of reagents, often forms different Cu^{I} derivatives [11,21]. Those arguments were the reason for exploring other areas of the Cu-DABCO-HCl composition diagrams to obtain the possible compounds in definite molar ratios of reagents.

There are six common synthetic methods of PNC and MOFs: microwave-assisted, mechanochemical, sonochemical, slow evaporation, electrochemical, and solvothermal [22–26]. Electrochemical synthesis has already proved to be an effective method for forming Cu^{I}-derivatives, because of such advantages: the absence of by-products and the possibility of growing high-quality crystals in one step [27]. Also, the electrochemical methods are considered as green and sustainable techniques for metalloorganic preparation, since they are relying on the use of the most convenient and easily available type of energy and known to be selective and atom-economic [28,29]. Using electrochemical synthesis with alternating current and varying the molar ratios of starting reagents in ethanol solvent, single crystals of two earlier unknown Cu^{I}-Cl-DABCO compounds (**I-II**) were obtained and characterized by single-crystal X-ray diffractometry and by Raman spectroscopy. However, the crystals of other previously published compounds appeared in this study by electrochemical synthetic work too, which is shown on the diagram (Figure 2). On the other hand, a solvothermal method is still more effective for forming compounds with complicated structural geometry, because of providing high activation energy and better solubility of some of the starting reagents, possibility to control thermodynamics and crystallinity [30]. It is still the most preferred [22,26] method being used in approximately 70% of published works on MOF materials. Moreover, this method could vary different synthetic parameters, such as temperature, solvent, reaction time, to optimize the nuclearity of the metal clusters, and porosity of metal-organic and inorganic frameworks. Using this alternative synthetic

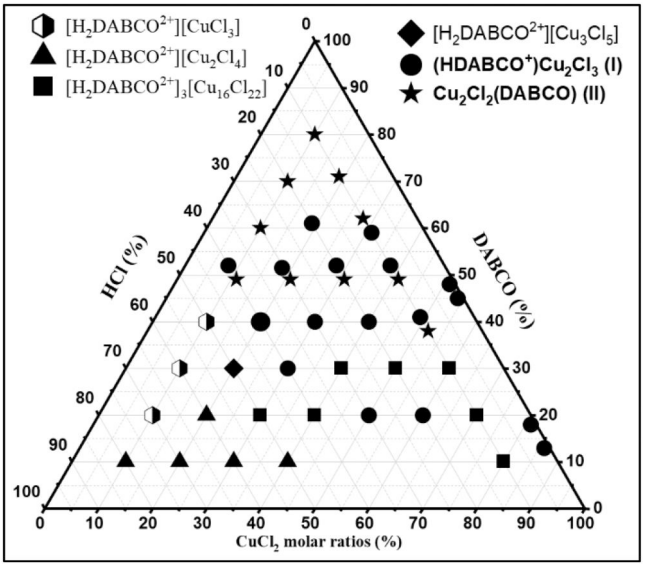

Figure 2. Composition space diagram of the CuCl–DABCO–HCl system, prepared by the electrochemical method. New compounds, prepared by this method, are marked in the legend by **bold**. This diagram is related to Table 1.

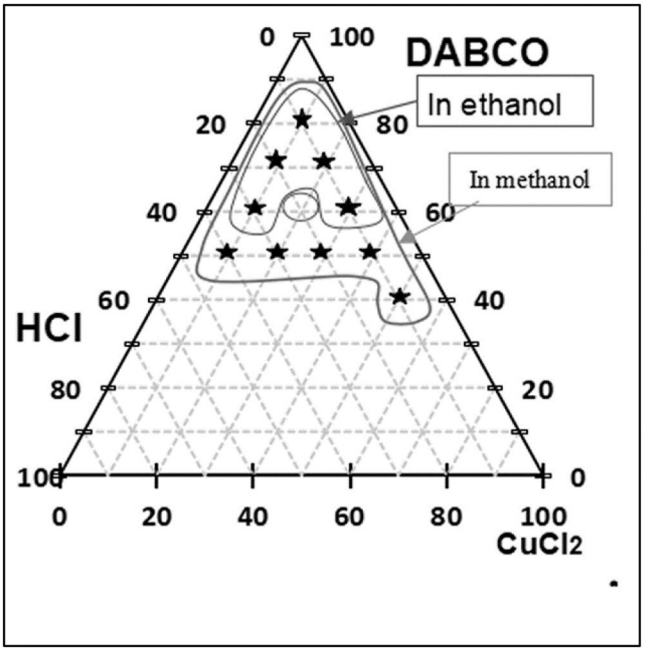

Figure 3. Formation ranges of the Cu_2Cl_2(DABCO) compound according to the electrochemical method in ethanol and methanol.

technique, an additional five compounds (**III-VII**) were obtained and studied (Figure 4). Together, they cover almost the whole CuCl-DABCO-HCl composition space diagram (Figure 5). The results are presented in this article.

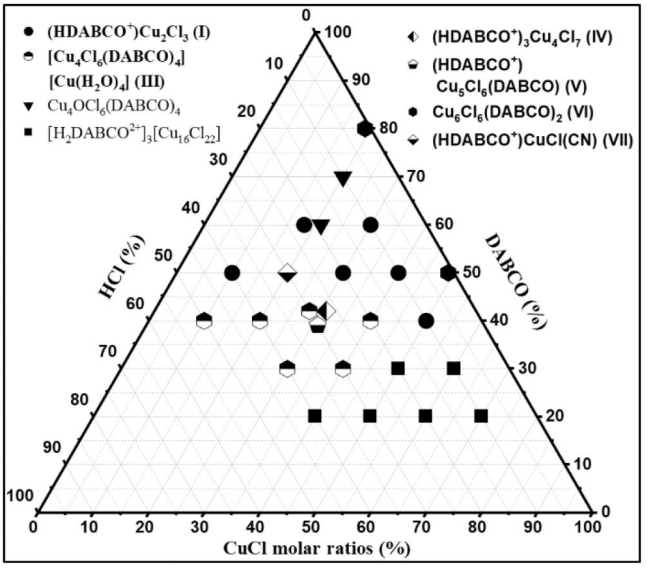

Figure 4. Composition space diagram of the CuCl–DABCO–HCl system, prepared by the solvothermal method. New compounds, prepared by this method, are marked in the legend by **bold.** This diagram is related to Table 1.

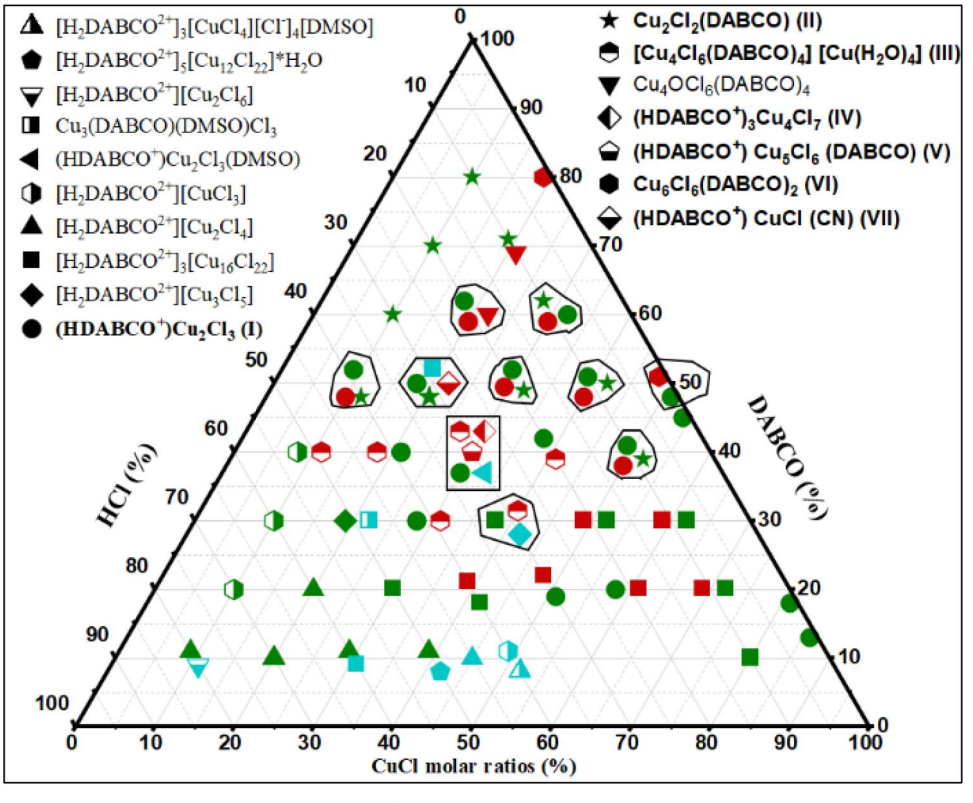

Figure 5. Composition space diagram of the **CuCl–DABCO–HCl system**, including previously published and new compounds, synthesized electrochemically and solvothermally. New compounds are marked in the legend by **bold**. This diagram is related to Table 1. **Point colors**: blue—previously published compounds; green—synthesized by electrochemical method compounds; red—synthesized by solvothermal method compounds.

2. Experimental part

All chemicals were of commercial origin: $CuCl_2{\cdot}2H_2O$ from Zorka Šabac (a.), copper powder (99.5%) from Merck, CuCl (98%) from TCI, $CuCl_2$, 1,4-diazabicyclo [2.2.2] octane (98%), ethanol (a.), hydrochloric acid 37% (ACS reagent) from Sigma-Aldrich, acetonitrile (99.9%) from Riedel-de Haën, and methanol (a.) from Carlo Erba.

2.1. Synthetic work

The experiments were carried out using two methods: solvothermal and electrochemical alternating current.

The experiments on electrochemical alternating current synthesis were performed using copper wires as electrodes and ethanol or methanol as solvents. All samples were placed in small test tubes with a volume of 5 mL. The electrodes (one is a spiral, the second is a straight rod inside the spiral) were inserted into the cork, immersed in the above solution, and an alternating current of 50 Hz with a voltage of 0.85 V was applied. The voltage was measured with a multimeter. Crystals of the compound **$(HDABCO^+)Cu_2Cl_3$ (I)** were obtained in the molar ratios $CuCl_2{\cdot}2H_2O$: DABCO: HCl shown in Table 1. Each sample was prepared by dissolving $CuCl_2{\cdot}2H_2O$ (10 mg, 0.0587 mmol) and approximate amounts of DABCO (in accordance with molar ratios of DABCO (20–60%), which are placed in Table 1) in ethanol (3 mL). A standard solution of HCl in ethanol was prepared by mixing 0.5 ml of 37% HCl and 20 mL of ethanol before preparing the samples. Selected amounts of this solution were added to the $CuCl_2{\cdot}2H_2O$–DABCO mixtures in accordance with the molar ratios of HCl (10–40%), described in Table 1. Over the next 3–5 days, numerous colorless prismatic crystals appeared on the electrodes and green precipitate on the bottom of the test tube as a by-product. This compound was also synthesized by the electrochemical technique without the presence of HCl in the samples, using $CuCl_2$: DABCO molar ratios marked on the DABCO axis in Figure 2, Figure 3, and Table 1.

Crystals of the compound **Cu_2Cl_2(DABCO) (II)** were obtained in the samples with molar ratios of $CuCl_2{\cdot}2H_2O$: DABCO: HCl depicted in Table 1. The standard solution of HCl in ethanol was added to the samples in accordance with HCl molar ratios (10–30%) described in Table 1. The amounts of $CuCl_2{\cdot}2H_2O$ (10 mg, 0.059 mmol), the alternating current, the voltage 0.85 V, and the volumes of the reaction mixtures (3 mL) were the same as for the synthesis of compound **I**. After 7 days, the pale-brown prismatic crystals appeared on the electrodes and a brown precipitate on the bottom of the test tube as a by-product.

The use of methanol instead of ethanol leads to a shift and expansion of the area on the composition space diagram where **Cu_2Cl_2(DABCO)** compound appears (Figure 4).

Crystals of **$[Cu(H_2O)_4][Cu_4Cl_6(DABCO)_4]$ (III)** were obtained by solvothermal synthesis performed in a 20-mL Teflon TM liner heated in a steel autoclave at 150 °C for 5 days. The reaction mixtures were prepared by mixing anhydrous $CuCl_2$ (100 mg, 0.744 mmol), copper powder (48 mg,0.744 mmol), and respective amounts of DABCO and HCl in accordance with the molar ratios presented in Table 1. Each reaction mixture was dissolved in 10 mL of ethanol. After slowly cooling down the temperature,

Table 1. Molar ratios of reagents used for the synthetic part, with the respective obtained compounds. New compounds are marked in **bold**. This table is related to the composition space diagrams in Figures 2–5.

Molar ratios %			Compounds synthesized by	
CuCl, Cu, $CuCl_2$	DABCO	HCl	Electrochemical method	Solvothermal method
10	10	80	*$[H_2DABCO^{2+}][Cu_2Cl_4]$ (1)	
20	10	70		
30	10	60		
40	10	50		
80	10	10	*$[H_2DABCO^{2+}]_3[Cu_{16}Cl_{22}]$ (1)	
10	20	70	*$[H_2DABCO^{2+}][CuCl_3]$ (1)	
20	20	60	*$[H_2DABCO^{2+}][Cu_2Cl_4]$ (1)	
30	20	50	*$[H_2DABCO^{2+}]_3[Cu_{16}Cl_{22}]$ (1)	
40	20	40		* $[H_2DABCO^{2+}]_3[Cu_{16}Cl_{22}]$ (1)
50	20	30	***$(HDABCO^+)Cu_2Cl_3$** (1)	
60	20	20		
70	20	10	*$[H_2DABCO^{2+}]_3[Cu_{16}Cl_{22}]$ (1)	
10	30	60	*$[H_2DABCO^{2+}][CuCl_3]$ (1)	
20	30	50	*$[H_2DABCO^{2+}][Cu_3Cl_5]$	
30	30	40	***$(HDABCO^+)Cu_2Cl_3$** (1)	***[Cu $(H_2O)_4$][Cu_4Cl_6(DABCO)] (1)**
40	30	30	*$[H_2DABCO^{2+}]_3[Cu_{16}Cl_{22}]$ (1)	
50	30	20		*$[H_2DABCO^{2+}]_3[Cu_{16}Cl_{22}]$ (1)
60	30	10		
10	40	50	*$[H_2DABCO^{2+}][CuCl_3]$ (1)	**[Cu_4Cl_6(DABCO)][Cu $(H_2O)_4$] (1)**
20	40	40	***$(HDABCO^+)Cu_2Cl_3$ (1)**	
30	40	30		**$(HDABCO^+)_3Cu_4Cl_7$ (1), $(HDABCO^+)$ Cu_5Cl_6(DABCO) (2), [Cu $(H_2O)_4$][Cu_4Cl_6(DABCO)] (1)**
40	40	20		***[Cu $(H_2O)_4$][Cu_4Cl_6(DABCO)] (1)**
50	40	10	***$(HDABCO^+)Cu_2Cl_3$ (1),**	**$(HDABCO^+)Cu_2Cl_3$(1)**
10	50	40	***Cu_2Cl_2(DABCO) (2)**	
20	50	30		[i] **$(HDABCO^+)$CuCl(CN) (3)**
30	50	20		**$(HDABCO^+)Cu_2Cl_3$ (1)**
40	50	10		
10	60	30	***Cu_2Cl_2(DABCO) (1, 2)**	
20	60	20	***$(HDABCO^+)Cu_2Cl_3$ (1)**	**$(HDABCO^+)Cu_2Cl_3$ (1),** $Cu_4OCl_6(DABCO)_4$ (1)
30	60	10	***Cu_2Cl_2(DABCO) (1,2)**	**$(HDABCO^+)Cu_2Cl_3$** $Cu_4OCl_6(DABCO)_4$ (1)
10	70	20		
20	70	10		
10	80	10		
20	80	0		[i] **$Cu_6Cl_6(DABCO)_2$ (1)**
50	50	0	**$(HDABCO^+)Cu_2Cl_3$ (1)**	
82	18	0		
87	13	0		

Notes.
*prepared using HCl standard solution in ethanol (methanol).
[i] prepared using CuCl.
Solvents for preparation.
1. Ethanol.
2. Methanol.
3. Acetonitrile.

the pale brown-crystals of the obtained compound and brown precipitate as a by-product were found at the bottom of the line.

The **$(HDABCO^+)_3Cu_4Cl_7$** (I**V**) compound was synthesized by the solvothermal method in 10 mL of ethanol and with the respective molar ratios of reagents (shown in Table 1), but with two changes:

- increased reagent amounts: $CuCl_2$ 200mg (1.488 mmol), copper powder 95 mg (1.488 mmol), and the respective increased amounts of DABCO and HCl in accordance with molar ratios Table 1;
- decreasing the working temperature to 130 °C.

Colorless plate crystals of the compound and small particles of copper powder were obtained at the bottom of the line after the synthetic work was completed.

The **$(HDABCO^+)Cu_5Cl_6(DABCO)$** (**V**) compound was synthesized by the solvothermal method at 130 °C in 10 mL of methanol. The reaction mixture was prepared by mixing 200 mg (1.488 mmol) of $CuCl_2$ and copper powder (95 mg, 1.488 mmol) with DABCO and HCl in accordance with the molar ratios in Table 1, and dissolving this mixture in methanol. After completing the synthetic work, plenty of yellow-block crystals free of any non-crystalline by-products were obtained at the bottom of the liner.

The **$Cu_6Cl_6(DABCO)_2$** (**VI**) compound was synthesized under solvothermal conditions at 150 °C using CuCl without the use of HCl. The reaction mixtures were prepared by mixing CuCl (74 mg, 0.75 mmol) with the corresponding amount of DABCO (molar ratios are shown in Table 1). Then, 10 mL of ethanol was added to dissolve the mixture. After finishing the synthesis, the colorless plate crystals were obtained at the bottom of the liner with no by-products.

The **$(HDABCO^+)CuCl(CN)$** (**VII**) compound was synthesized under solvothermal conditions at 170 °C for 4 days using CuCl and copper powder, and acetonitrile (10 mL, 191.5 mmol) as solvent with a CuCl: DABCO: HCl molar ratio described in Table 1. Reaction was prepared by mixing 75 mg (0.758 mmol) of CuCl with respective amount of 37% HCl (Table 1), and 2 mL of acetonitrile was added to the mixture. Then, the corresponding amount of DABCO (taken in accordance with the molar ratio in Table 1) was dissolved in 8 mL of acetonitrile and added to the mixture. After completion of the reaction and slow cooling of the autoclave to room temperature, the irregular-shaped colorless crystals of compound **VII** and the dark-brown precipitate as a by-product were found at the bottom of the liner.

The crystals of all the obtained compounds are stable in ambient conditions in the air. The chemical structure of the obtained crystalline compounds was determined using single-crystal X-ray diffraction. Raman spectroscopy was used to detect the changes in characteristic peaks of organic fragments in each compound.

2.2. X-ray structure determination

Single-crystal X-ray data were collected on a Gemini A diffractometer equipped with an Atlas CCD detector, using graphite monochromatic CuKα radiation. The data were processed using the CrysAlisPro software suite program [31] package. Analytical absorption corrections were applied to all the datasets. All structures were solved using the dual-space algorithm of the SHELXT [32] program implemented in Olex crystallographic [33] software. Structure refinement was performed with the SHELXL-2014 software [32]. Refinement converged at relatively low *R*-factor values (Table 1). Careful inspection of the data using the TwinRotMat procedure implemented in Platon

software has shown the presence of inversion twinning for the **I** and **III** compounds [34]. Non-merohedral twinning found for the datasets of **II** and **VI** compounds was resolved by generating an HKLF5 file using the CrysAlisPro software package. The positions of hydrogen atoms from the amino groups were found on a difference Fourier map, their positional and isotropic thermal parameters were freely refined, and other hydrogen atoms were placed in ideal positions and refined as riding atoms with relative isotropic displacement parameters. Crystallographic data for the structures have been deposited with the Cambridge Crystallographic Data Center, **CCDC** Nos 2494278 (**I**), 2494276 (**II**), 2494279 (**III**), 2494282 (I**V**), 2494280 (**V**), 2494277 (**VI**), and 2494281 (**VII**). Copies of data can be obtained, free of charge, on application to the Director, CCDC, 12 Union Road, Cambridge CB2 1 EZ, UK (fax: +44 1223 336033 or e-mail: deposit@ccdc.cam.ac.uk). The figures were prepared using the DIAMOND 4.6 software [35]. Topological analysis was performed using the TopCryst web service (http://topcryst.com).

2.3. Raman spectroscopy

Raman spectra with a resolution of 0.5 cm^{-1} were recorded at room temperature on a HORIBA JOBIN YVON LabRam-HR spectrometer equipped with the Olympus BXFM-ILHS microscope. Samples were excited by a He-Ne laser's 632.8 nm and 532 nm emission lines in the 100–4000 cm^{-1} spectral region. Before data recording, the instrument scale was calibrated using a silicon polycrystalline plate (a characteristic band at 521 cm^{-1}).

3. Results and discussions

3.1. Composition space diagram

The 2-D composition space diagram of the CuCl–DABCO–$HCl_{aq.}$ system was established for several concentrations (0.02, 0.045, 0.15 mol/l) of copper salt at room temperature using alternating current 50 Hz 0.8–0.85 V and ethanol as solvent (Figure 2).

As expected, the formation of H_2DABCO^{2+} cupro(I)chlorides was observed in strongly acidic media. The main product in this range is the $[H_2DABCO^{2+}]$ $[Cu_2Cl_4]$ salt, which contains an infinite $\{[Cu_2Cl_4]^{2-}\}_n$ anionic chains. The formation of $[H_2DABCO^{2+}]$ $[CuCl_3]$ with isolated $[CuCl_3]^{2-}$trigonal anions and $[H_2DABCO^{2+}]$ $[Cu_3Cl_5]$ with complex $\{[Cu_3Cl_5]^{2-}\}_n$ anions was also observed in the HCl-rich region (Figure 2). All the above compounds were also obtained by the electrochemical method [11,18].

The formation of a 3-D $[Cu_{16}Cl_{22}]^{6-}$ cupro(I)chloride framework [14] containing diprotonated H_2DABCO^{2+} counter ions was observed in a rather narrow range of DABCO concentration. Crystals of this compound, which were initially obtained under solvothermal conditions (Figures 1 and 4), frequently occurred as (by-)products of electrochemical syntheses (Figures 2 and 5).

The formation of 2-D $[Cu_{12}Cl_{22}]^{10-}$ layers was observed earlier [11] in a very narrow range of reagent ratios. The corresponding $[H_2DABCO^{2+}]_5[Cu_{12}Cl_{22}]$ compound also appears in an HCl-rich area.

A decrease in the acidity of the medium leads to the appearance of $HDABCO^{+}$ cations. Surprisingly, in contrast to a large number of H_2DABCO^{2+} cupro(I)chlorides, the

only $(HDABCO^+)Cu_2Cl_3$ salt was obtained in a relatively broad region of the diagram (Figure 2). Its structure consists of monoprotonated $HDABCO^+$ cations and infinite $\{Cu_2Cl_3^-\}_n$ chains. It should be noted that this compound also forms in samples without HCl (Figure 2). The partial hydrolysis of the starting $CuCl_2$ is probably responsible for the formation of the protonated DABCO form. Previously, the only one $HDABCO^+$ cupro(I) chloride, namely $(HDABCO^+)Cu_2Cl_3(DMSO)$, was described [9].

In the region with the lowest acidity, the compound appears with a neutral tryethylenediamine which serves as a bridging ligand in $Cu_2Cl_2(DABCO)$. Changing the solvent to methanol expands the formation area, as shown in Figure 3.

The most pronounced influence of the CuCl:HCl ratio was observed at an isoline of 20 mol.% DABCO (Figure 2). Decreasing the acidity leads to a gradual change of the inorganic fragment from isolated $CuCl_3^{2-}$ to 1-D chains $\{[Cu_2Cl_4]_n\}^{2n-}$ to 3-D-$[Cu_{16}Cl_{22}]^{6-}$ framework (all with H_2DABCO^{2+} di-cations). A further reduction in acidity leads to the $(HDABCO^+)Cu_2Cl_3$ salt.

The 2-D composition space diagram of the $CuCl_2$–DABCO–$HCl_{aq.}$–EtOH system under solvothermal conditions is established for a $CuCl_2$ concentration (0.074 mol/l) at 150 °C (Figure 4).

In the solvothermal method (Figure 4), one can see a shift in the appearance of the crystals of the $(HDABCO^+)Cu_2Cl_3$ compound in the area with a higher DABCO concentration. Changing the solvent to acetonitrile in this area leads to the formation of Cu-CN chains instead of Cu_2Cl_3 chains, which include monoprotonated $HDABCO^+$ cations and terminal chloride anions as side substituents.

At high DABCO concentrations (Figure 4), crystals of an undesirable Cu(II) compound with the composition $Cu_4OCl_6(DABCO)_4$ occur. The crystal structure contains inorganic Cu_4OCl_6 clusters connected by neutral DABCO ligands as linkers, forming a known metal-organic framework MFU-5 [36].

The copper mixed-valent metal-organic framework $[Cu^{II}(H_2O)_4][Cu^{I}_4Cl_6(DABCO)_4]$ appears in the range of relatively low concentrations of $CuCl_2$ (10–50%). The HCl, used as the reagent, and ethanol, used as a solvent, contain water, which also acts as a reactant in the compound formation. Thus, the molar ratio of HCl in preparation of the samples is relatively low—20–50% (Table 1, Figure 4), where the ratio of water to hydrogen chloride is 63:37 or ~3:2. The amount of water in ethanol is 0.4 mL (4% of 10 mL of ethanol). This water plays a significant role in the framework formation. The use of a lower temperature for the synthesis (130 °C) and higher concentrations of the reagents (x2) at the same molar ratios leads to the appearance of $(HDABCO^+)_3Cu_4Cl_7$ crystals, containing three monoprotonated $HDABCO^+$ cations coordinated to the negatively charged inorganic oligomer $[Cu_4Cl_7]^{3-}$. The presence of water from HCl and ethanol (as it was in the formation of compound III) leads to the inclusion of an isolated water molecule into the crystal structure of this compound. The use of methanol instead of ethanol in this region under the same conditions leads to the formation of another compound $(HDABCO^+)Cu_5Cl_6(DABCO)$, consisting of unprotonated DABCO and monoprotonated $HDABCO^+$ coordinated to the negatively charged inorganic cluster $[Cu_5Cl_6]^-$.

In the absence of HCl, the compound $Cu_6Cl_6(DABCO)_2$, consisting of $[Cu(DABCO)_2]^+$ complex cations and negatively charged inorganic clusters $[Cu_5Cl_6]^-$, was obtained (Figures 4 and 5).

Increasing the acidity at high temperature leads to the reaction of the molecules of solvent (ethanol, methanol) with DABCO molecules *via* amine groups, forming N-$X_{(1;2)}$ $DABCO^{1+;2+}$ (X = Et, Me) ligands, which have the role of organic mono- or di-cations. These ligands form additional Cu-Cl-polyamine coordination compounds, which are the subject of separate research.

As a result, the Cu-Cl–DABCO-containing coordination compounds, synthesized by electrochemical and solvothermal methods, cover almost the entire Cu-Cl–DABCO composition space diagram (Figure 5).

3.2. Influence of solvent and electrical parameters on the formation of definite products by the electrochemical method

All the syntheses were prepared in the polar solvents: ethanol and methanol. Reactions were carried out in a 5-mL glass test tube using 3 mL of each solution. Small amounts of reagents $CuCl_2 \cdot 2H_2O$ (0.0587 mmol) and DABCO (0.0587–0.469 mmol) were used to prepare the samples to decrease the formation of powder.

The molecule of DABCO has a high nucleophilicity because the amine groups are unhindered. The first pKa of DABCO in protonic solvents is 8.8 (one amine group is protonated). The second pKa is 3, which is responsible for the protonation of both amine groups. $(HDABCO^+)Cu_2Cl_3$ appeared in the reaction solutions with a pH of 4.5–6. That is why we obtained a chemical structure with monoprotonated DABCO. $Cu_2Cl_2(DABCO)$ appeared in the reaction solutions with pH 7–8.5, which is close to the pKa_1, and the chemical structure consists of unprotonated DABCO [37].

Electric current influences the velocity of electrochemical reactions and crystal formation. The minimum voltage required for the synthetic work was measured with a multimeter at 0.15 V, indicating the redox potential of Cu^{2+}/Cu^+ [38]. Increasing the voltage accelerates the reaction. However, when the reaction is too fast, it decreases the crystal quality. Practically, it was found that applying more than 1 V gives a very poor crystallinity. The optimal voltage was 0.7–0.9 V, facilitating growing crystals with good diffraction during the most optimal time (2–7 days).

3.3. Crystal structures

Compound $(HDABCO^+)$ Cu_2Cl_3 (**I**) crystallizes in the orthorhombic $P2_12_12_1$ space group (Table 2) as colorless prismatic crystals (Fig. S1a). The crystal structure contains a monoprotonated $HDABCO^+$ cation, coordinated to the Cu1 ion *via* an unprotonated N1 center with Cu1–N1 bond distance of 2.059(5) Å (Figure 6 and Fig. S1b). Both crystallographically independent Cu1 and Cu2 centers are four-coordinated (Fig. S1c). The Yang geometry $\tau'4$ parameter values of 0.93 and 0.68, respectively, indicate an almost regular tetrahedral environment for Cu1 and a distorted tetrahedral surrounding for Cu2. The previously published $(HDABCO^+)$ $Cu_2Cl_3(DMSO)$ compound, prepared in DMSO, has an almost regular tetrahedral environment around both copper centers,

Table 2a. The crystal data and refinement parameters of the compounds **I**, **II**, and **III**.

Compound	I	II	III
CCDC number	2494278	2494276	2494279
Chemical formula	$C_6H_{13}Cl_3Cu_2N_2$	$C_6H_{12}Cl_2Cu_2N_2$	$C_{24}H_{48}Cl_6Cu_6N_8{\cdot}12H_2O$
M_r	346.61	310.16	1190.16
Crystal system, space group	Orthorhombic, $P2_12_12_1$	Monoclinic, $P2_1/c$	Cubic, $I^-4\,3\,m$
Temperature (K)	150		
a, b, c (Å)	9.2579 (4), 13.8136 (5), 8.3137 (4)	12.7214 (6), 11.9707 (8), 6.0248 (4)	13.0392 (2)
α, β, γ	90, 90, 90	90, 93.897(4), 90	90,90,90
V (Å^3)	1,063.20 (8)	915.36 (10)	2,216.93 (10)
Z	4	4	2
Radiation type	Cu $K\alpha$		
μ (mm^{-1})	11.50	10.63	6.64
Crystal size (mm)	0.32 × 0.14 × 0.11	0.27 × 0.11 × 0.07	0.23 × 0.21 × 0.15
T_{min}, T_{max}	0.201, 0.455	0.136, 0.580	0.616, 1.000
No. of meas., inde and obser. [I > 2σ(I)] reflect.	4661, 2186, 1900	4975, 1881, 1351	22064, 468, 425
R_{int}	0.049	0.050	0.089
$(\sin\theta/\lambda)_{max}$ (Å^{-1})	0.630	0.629	0.630
$R[F^2 > 2\sigma(F^2)]$, $wR(F^2)$, S	0.035, 0.084, 1.07	0.048, 0.132, 1.05	0.054, 0.161, 1.12
No. of reflections	2,186	1,881	468
No. of parameters	123	109	50
No. of restraints			1
H-atom treatment	H atoms treated by a mixture of independent and constrained refinement	H-atom parameters constrained	
$\Delta\rho_{max}$, $\Delta\rho_{min}$ (e Å^{-3})	0.63, −0.52	1.28, −0.61	0.68, −0.43
Absolute structure	Refined as an inversion twin		Refined as an inversion twin
Absolute structure parameter	0.44 (5)		0.50 (14)

with Yang parameters of 0.94 and 0.99, respectively [9]. Due to the bridging function of the chloride ions, infinite slightly wave-like cupro-chloride chains with 2,2,4C4 topology running along the b-axis appear (Fig. S1c). The Cl1 atom acts as a single bridge between Cu1 and Cu2 centers (Cu1–Cl1–Cu2 angle is 140.6(1) °), whereas Cl2 and Cl3 ions form a rhomb with two metal cations (Cl2–Cu2–Cl3 and Cl2–Cu1^{I}–Cl3 angles are ∼74°). Such diversity in bridging mode is reflected in noticeable differences in Cu–Cl distances. The lengths of Cl1–Cu bonds vary from 2.1864(16) to 2.3264(17) Å, while the Cl2–Cu and Cl3–Cu distances are longer, ranging from 2.268(2) to 2.453(2) Å. Each Cl1 center also forms a weak hydrogen bond with an H(C6) atom of DABCO from another neighboring chain (Cl1 … H6 2.913 Å, Cl1 … H6–C6 angle 125.273°). This H-bond is noticeably longer than an analogous bond of ($HDABCO^+$) Cu_2Cl_3(DMSO) compound [9] with Cl … H distance 2.660 Å. Each H(N2) atom forms 2 hydrogen bonds with 2 chlorine Cl2 and Cl3 centers from another neighboring chain (Cl2 … H2 2.632 Å, angle 126.397 °, Cl3 … H2 2.652 Å, angle 133.759 °). These H interactions hold the chains together. The $HDABCO^+$ fragment has an untwisted conformation (Fig. S1d). The crystal structure shows that the H^+(N) atom is alternately bound to one of two nitrogen atoms from two neighboring chains when hydrochloric acid is present in the starting mixture of reagents. This disorder was not observed in samples obtained without HCl.

Table 2b. (*continuation*). The crystal data and *cif* parameters of the compounds **IV**, **V**, **VI**, and **VII.**

Compound	IV	V	VI	VII
CCDC number	2494282	2494280	2494277	2494281
Chemical formula	$C_{18}H_{39}Cl_7Cu_4N_6{\cdot}0.2H_2O$	$C_{12}H_{25}Cl_6Cu_5N_4$	$C_{12}H_{24}Cl_6Cu_6N_4$	$C_7H_{13}ClCuN_3$
M_r	846.42	755.76	818.29	238.19
Crystal system, space group	Monoclinic, $P2_1/m$	Monoclinic, $P2_1/n$	Monoclinic, $P2_1/n$	Monoclinic, $P2_1/n$
Temperature (K)	150			
a, *b*, *c* (Å)	8.2662 (2), 9.5494 (4), 18.6837 (5)	12.8550 (2), 10.6411 (2), 16.5017 (3)	12.2894 (7), 10.7480 (6), 17.8830 (7)	8.3768 (4), 8.9608 (5), 11.9080 (5)
α, β, γ	99.782 (3)	105.194 (2)	90, 104.882 (4), 90	97.427 (4)
V (Å^3)	1,453.40 (8)	2,178.38 (7)	2,282.9 (2)	886.35 (8)
Z	2	4	4	4
Radiation type	Cu *K*α			
μ (mm^{-1})	9.40	12.23	12.62	5.81
Crystal size (mm)	0.2 × 0.13 × 0.06	0.53 × 0.35 × 0.17	0.31 × 0.27 × 0.14	0.25 × 0.18 × 0.12
T_{min}, T_{max}	0.624, 0.846	0.193, 0.458	0.075, 0.325	0.347, 0.579
No. of meas., inde, and obser. [I > 2σ(I)] reflect.	13437, 3206, 2659	22888, 4527, 3751	18832, 4128, 3450	7496, 1827, 1584
R_{int}	0.042	0.046	0.071	0.033
$(\sin\theta/\lambda)_{max}$ (Å^{-1})	0.631	0.630	0.631	0.630
$R[F^2 > 2\sigma(F^2)]$, $wR(F^2)$, *S*	0.038, 0.099, 1.05	0.050, 0.150, 1.07	0.049, 0.138, 1.06	0.037, 0.104, 1.07
No. of reflections	3206	4527	4128	1827
No. of parameters	226	270	1	113
No. of restraints	7			
H-atom treatment	H atoms treated by a mixture of independent and constrained refinement		H-atom parameters constrained	H atoms treated by a mixture of independent and constrained refinement
$\Delta\rho_{max}$, $\Delta\rho_{min}$ (eÅ^{-3})	0.60, −0.53	1.60, −1.80	1.28, −0.68	1.16, −0.32

Compound Cu_2Cl_2(DABCO) (**II**) crystallizes in the monoclinic $P2_1/c$ space group (Table 2). The organic component of the crystal structure is a neutral DABCO ligand, which acts as a bridge between two copper centers, with Cu–N distances of 1.986(5) and 1.991(5) Å (Figure 7 and Fig. S2b). Each metal ion is coordinated by a nitrogen atom from DABCO and two bridging chloride ions, with Cu–Cl distances of 2.1896(18)–2.4353(19) Å (Figure 7). The inorganic part of the structure consists of infinite $(CuCl)_n$ zig-zag chains running along the c-axis (Figure 7 and Figure 2d). These chains are connected by DABCO linkers into 2D zig-zag layers, which are sandwich-oriented to each other (Figure 2c). The DABCO fragment has a left-twisted conformation (Fig. S2e).

The compound $[Cu(H_2O)_4][Cu_4Cl_6(DABCO)_4]$ **(III)** crystallizes in the cubic I $\bar{4}$ 3 m group (Table 2) as pale-brown cubic twinned crystals (Fig. S3a). The crystal structure consists of a 3-D anionic metal-organic framework (Figure 8.2 and Fig. S3c), composed of neutral DABCO linkers between inorganic $Cu_4Cl_6^{2-}$ clusters, which exhibit bcu, 8/4/c1, and sqc3 topologies, and $[Cu^{II}(H_2O)_4]$ square-planar cations (Figure 8.1, Fig. S3b, and Fig. S3c), which serve as inorganic hosts and structure-directing agents for the framework. Hosts occupy voids in the framework with approximate dimensions $6.854_{\times}7.173_{\times}7.572$ Å (Figure 8.2). Due to partial occupancies of Cu^{II} center (44%) and oxygens (50%), we could conclude that only approximately half of the voids are occupied by inorganic hosts. Each Cu1 and Cu2 ion is coordinated by a nitrogen atom of DABCO, with Cu–N distances of 2.159(15) and 1.98(3) Å, respectively (Fig. S3b), and three chlorine atoms with Cu–Cl bond lengths of 2.285(4)–2.3678(16). Cu-Cu interactions with short distances Cu1-Cu2 2.16(2) and Cu3-Cu2 2.678(12) also exist, which is confirmed by high luminescence [39] when trying to observe Raman spectra. The τ_4 parameter values for Cu1 and Cu2 are 1 and 0.99, respectively, indicating a regular tetrahedral environment for these coordination centers. The τ_4 parameter value for Cu4 is 0, indicating a regular square-planar geometry of the coordination environment.

The compound $(HDABCO^+)_3Cu_4Cl_7$ **(IV)** crystallizes in the monoclinic $P2_1/m$ space group (Table 2) as thin, plate-like colorless crystals (Fig. S4a). The asymmetric unit contains three monoprotonated $HDABCO^+$ cations, each coordinated to three Cu metal centers *via* unprotonated N atoms (Figure 9, Fig. S4b), with Cu–N distances of 2.077(3)–2.140(3) Å, and a three-coordinated Cu2 atom surrounded solely by chlorine atoms. The coordination around each of Cu1, Cu3, and Cu4 copper centers is completed to fourfold by three chloride ligands, with Cu–Cl distances of 2.2819(13)–2.5013(14) Å. The τ'_4 parameters for each four-coordinated metal center are 0.9–0.93, indicating an almost regular tetrahedral environment. Due to the bridging function of the chloride ligands, the inorganic component forms an inorganic oligomer, Cu_4Cl_7, with 1M2-1 topology, which is negatively charged and oriented along the c-axis (Fig. S4c). The DABCO fragment N1–N2 exhibits untwisted D_{3h} symmetry. Disordered parts of other DABCO moieties adopt twisted conformations, but the ordered parts correspond to the untwisted D_{3h} symmetry (Fig. S4d and Fig. S4e). A high peak of electron density appeared after the structural model was completed. Taking into account the electroneutrality of the whole model and the distance of the above peak of electron density to the closest hydrogen atom of 2.34(2), which is usual for H … O hydrogen

bonds, this peak was associated with an isolated H_2O molecule. The source of water was probably an aqueous solution of HCl and ethanol. Refined occupancy of this oxygen atom is 0.15, making it impossible to determine the positions of the H atoms. However, the presence of isolated water was not confirmed by Raman spectroscopy (Figures 11).

Compound $(HDABCO^+)Cu_5Cl_6(DABCO)$ **(V)** crystallizes in the monoclinic *P2₁/n* space group (Table 2) as yellow block crystals (Fig. S5a). Its crystal structure contains Cu_5Cl_6 anionic oligomers composed of two tetra-coordinated Cu4 and Cu5 metal centers connected by three twofold coordinated Cu bridges (Figure 10). The Cu4 center is coordinated, besides three chloride anions, by the unprotonated N atom of the $HDABCO^+$ cation (Cu5–N1 2.078(3) Å). In contrast, the Cu5 atom is bound to a neutral DABCO ligand *via* the N3 center (Cu5–N3 2.125(3) Å). Both DABCO fragments exhibit left-twisted $D_3(S)$ conformation (Fig. S5e and Fig. S5f). The Cu–Cl bonds for the tetra-coordinated metal centers range from 2.3411(11) to 2.3947(12) Å, while the Cu–Cl distances for the two-coordinated copper centers are 2.1327(14)-2.614(13) Å. The $\tau'4$ parameter values for Cu4 and Cu5 are 0.89, indicating an almost regular tetrahedral environment around these coordination centers. The Cu_5Cl_6 clusters have a 2C1 topology. All bridging metal centers are disordered over two positions with occupancies of 84% and 16%, respectively. These organic–inorganic hybrid coordination ensembles are oriented along the 001 direction (Figure 10, Fig. S5c) due to the presence of N-H … N hydrogen bonds with distances 1.752 Å between them. These ensembles are also held together into an H-bonded network *via* C-H … Cl hydrogen bonds with distances around 2.860 Å (Fig. S5d).

Compound $Cu_6Cl_6(DABCO)_2$ **(VI)** crystallizes in the monoclinic $P2_1/n$ group (Table 2) as colorless plate crystals (Fig. S6a). The crystal structure consists of infinite chains running along the c-axis (Figure 10.2, Fig. S6c, S6d, S6e), consisting of Cu_5Cl_6 clusters with 2,6-C1 topology (Fig. S6b and S6c) connected by DABCO–Cu–DABCO bridges (Figure 11). These chains are held together due C-H … Cl hydrogen bonds with distances 2.679–2.777 Å (Fig. S6d, S6e). Each Cu_5Cl_6 cluster is composed of a pair of tetra-coordinated Cu4 and Cu5 centers linked by three $CuCl_2$ bridges (Figure 11). Cu4-N and Cu5-N bond distances are 2.095(5) and 2.114(5) Å, respectively. The Cu–Cl distances around two-coordinated Cu1, Cu2, and Cu3 centers are 2.049(5)-2.238(5) Å, and the Cu–Cl bond lengths around tetra-coordinated Cu4 and Cu5 (Fig. S6b) are noticeably longer (2.3294(17)–2.4167(17) Å). τ_4 parameter values of Cu4 and Cu5 are 0.91 and 0.92, respectively, indicating the almost regular tetrahedral surrounding of these coordination centers. The neutral bridging DABCO fragments exhibit right-twisted $D_3(R)$ conformation (Fig. S6f).

Compound $(HDABCO^+)CuCl(CN)$ **(VII)** crystallizes in the monoclinic *P2₁/n* space group (Table 2). The chemical structure contains a monoprotonated $HDABCO^+$ cation, coordinated to the Cu1 ion *via* the unprotonated N1 of DABCO (Figure 12 and Fig. S7b) with a distance of 2.275(2) Å. The coordination center Cu1 is four-coordinated—it also coordinates two bridging cyanide ligands through Cu–C3/N3 and Cu–C4/N4 bonds with distances of 1.957(3)–1.960(3) Å, and a terminal chloride ion with a Cu – Cl distance of 2.4822(7) Å. $\tau4$ and $\tau'4$ parameter values of 0.88 and 0.82, respectively,

Table 3. Raman-spectra peaks of pure DABCO and DABCO-peaks in new **Cu^{I}-Cl-DABCO** compounds.

Compounds	In-δ (C-N-C)	Out-υa (N-C)	In-υs (N-C)	υs (C-C) In-υs (N-C)	υa (C-C) In-γt (CH2)	υs (C-C) In-υs (N-C) In-δs (N-C)	υa (C-C) In-υa (N-C) In-γt (CH2)	In-γs (CH2)	V_S CH	Vas CH
$(HDABCO^+)Cu_2Cl_3$	415	560	621	799	898	1021	1054	1457	2957	2986
$Cu_2Cl_2(DABCO)$	420	578	648	812	924	1009	1054	1453	2935	2969
$Cu_6Cl_6(DABCO)_2$	422	569	618	804	858	1011	1061	1454	2881	2943
$(HDABCO^+)$ $Cu_5Cl_6(DABCO)$	426	550	645	810	918	994	1057	1465	2893	2953
$(HDABCO^+)_3Cu_4Cl_7$	420	520	644	807	918	1017	1056	1465	2893	2953
$(HDABCO^+)$ CuCl (CN)	462	474	611	810	902	1010	1053	1461	2960	2980
DABCO	434	579	596	806	894	972	1062	1456	2871	2938

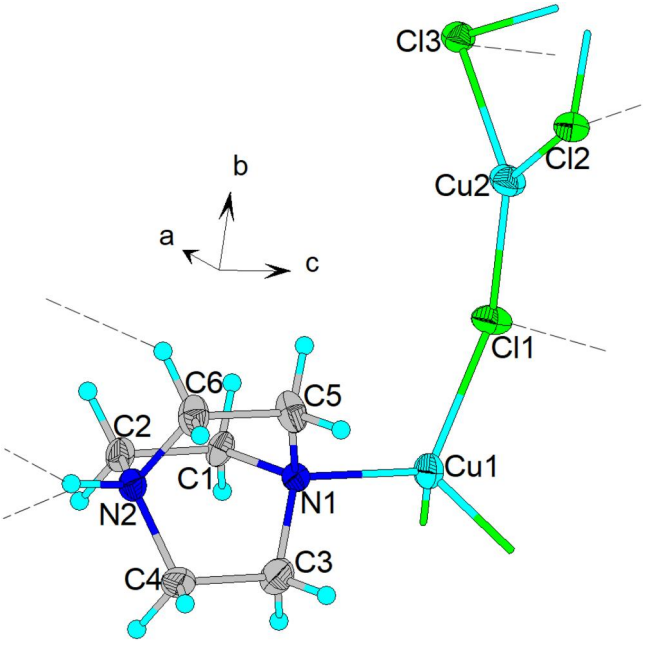

Figure 6. $HDABCO^+$ monocation coordinated with $[Cu_2Cl_3]_n$ inorganic chain in the compound **$(HDABCO^+)Cu_2Cl_3$**.

indicate a slightly distorted tetrahedral environment for Cu1. Due to the bridging function of the cyanide ligands, infinite cupro-cyanide chains with 2C1 topology run along the b-axis ([010] direction), with a 50/50 probability of Cu–CN and Cu–NC units (Fig. S7c). The H^+(N2) atom from the other side of DABCO forms a hydrogen bond with the Cl1 center from the neighboring chain. Each Cl center also forms a hydrogen bond with an H(N3) atom of DABCO from another neighboring chain (Cl1 … H3 distance 2.184 Å, Cl1 … H3–N3 angle 167.696°). The $HDABCO^+$ fragment has $D_3(S)$ conformation, which is left-twisted (Fig. S7d).

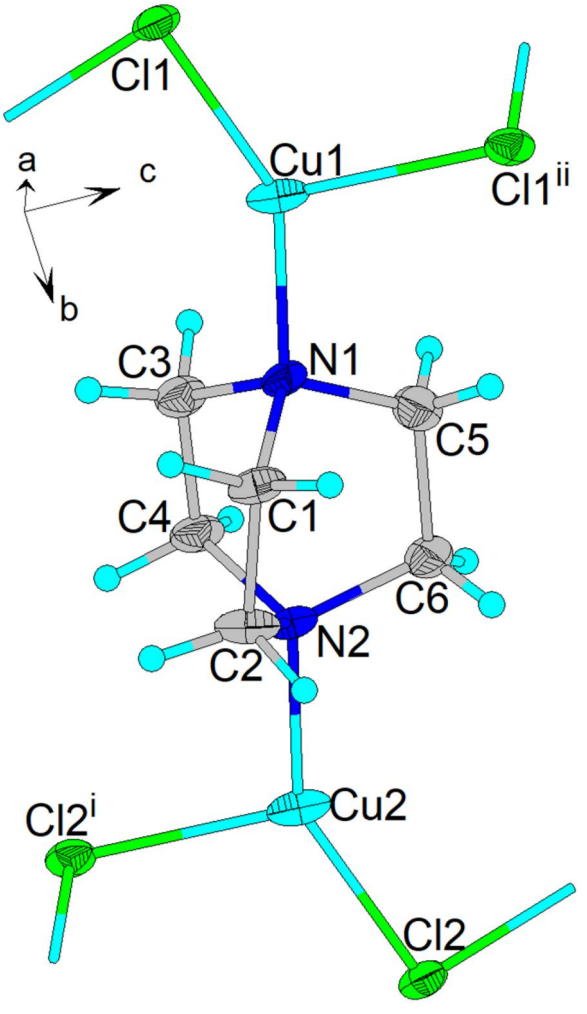

Figure 7. A neutral DABCO serves as a bridge between 2 inorganic [CuCl]n chains in the compound **Cu_2Cl_2(DABCO)**.

3.4. Raman spectra

A group of peaks 420, 560, 601, 803, 893, 977, 1056, and 1461 cm^{-1} observed in the Raman spectra of compounds **I**, **II**, **IV**, **V**, **VI**, and **VII** almost coincide with the spectra of pure DABCO (Table 3), as they originate from the organic part.

The v_s (NH) mode was found at 3,005–3,020 cm^{-1} in the two compounds (**I** and **VII**) with monoprotonated $HDABCO^+$ cations (Figures 13, S15). However, this peak is absent in the Raman spectra of compounds **IV**–**V**, which also contain $HDABCO^+$ cations (Fig. S11-12). In the spectrum of (I), it is represented as a peak, separated from the v_s- and v_{as}-(CH) mode group of peaks. In the case of VII, it overlaps the v_{as} (CH) peak, causing a visible peak asymmetry of the 2,964 cm^{-1} peak (Figure 15).

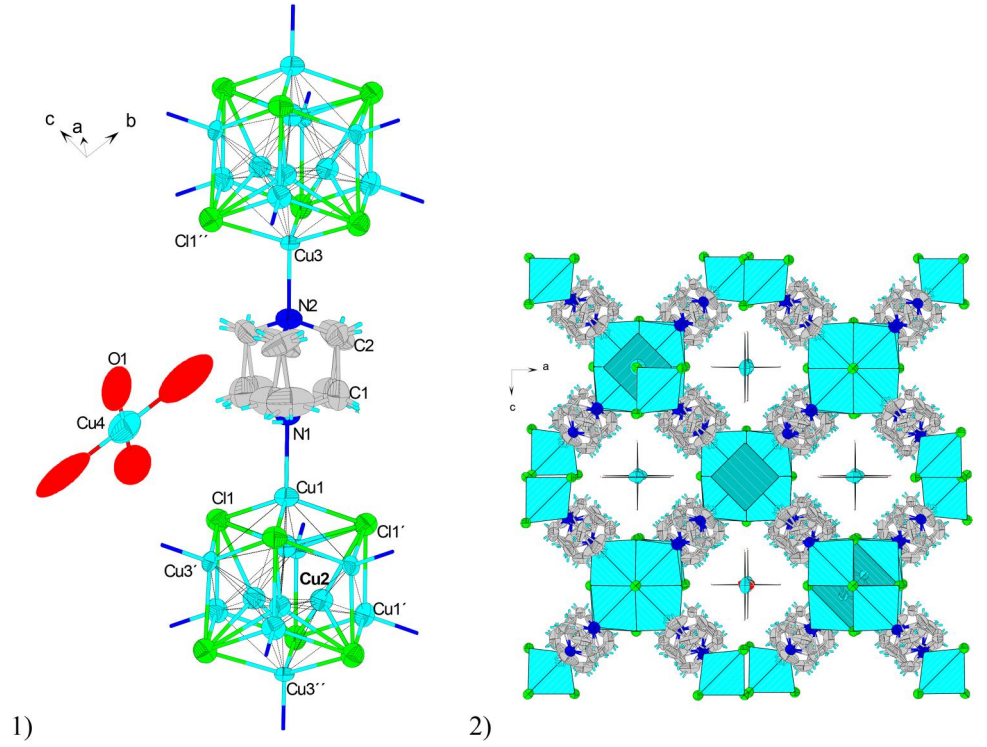

Figure 8. Organic-inorganic fragment **[Cu_4Cl_6(DABCO)]** with aqua complex **[$Cu(H_2O)_4$]** (1), of the metal-organic framework **[$Cu(H_2O)_4$][Cu_4Cl_6(DABCO)]** (2). For better image clarity, Cu-Cu interactions are dashed, and protons are omitted.

Peaks of ν_s and ν_{as} vibrations of C-H bonds in compounds **IV**–**VI** almost coincide (Fig. S11-13) with pure DABCO (Figures 8). However, these peaks are blue-shifted in the compounds **I**–**II** (Figures 9 and 10).

The peaks found at 235–300 cm^{-1} could be assigned to the ν_s mode of the Cu-Cl bond. For compounds with simple Cu_2Cl_3 or CuCl fragments (**I**, **II**, **VII**), it is represented by a number of closely located weak peaks, which correspond well with an assortment of Cu-Cl contacts (Figure 13,15). Tetranuclear Cu_4Cl_7 oblong oligomer and pentanuclear Cu_5Cl_6 clusters of the compounds **IV–VI** demonstrate this mode as a single strong peak (Figure 14) at 280–290 cm^{-1}.

It was problematic to observe the Raman spectrum of the **[$Cu(H_2O)_4$][Cu_4Cl_6(DABCO)]** compound because of the high luminescence of the crystal, which appeared during the observation. This luminescence appears due to the shorter ($\leq$ 2.80 Å) Cu-Cu interactions of Cu^I in the Cu_4Cl_6 clusters [39].

Besides the typical peaks of DABCO fragments, the compound **($HDABCO^+$)CuCl(CN)** also has a very strong scattering peak at 2,103 cm^{-1} that corresponds to the ν_s vibrations related to CN groups (Figure 15). The vibrations in CN ligands probably also overlap with N-C vibrations of DABCO. It induces a red shift in out-of-plane asymmetric stretching vibrations of N-C bonds (Out-υa (N-C) mode) from 560 to 580 cm^{-1} to 474 cm^{-1}.

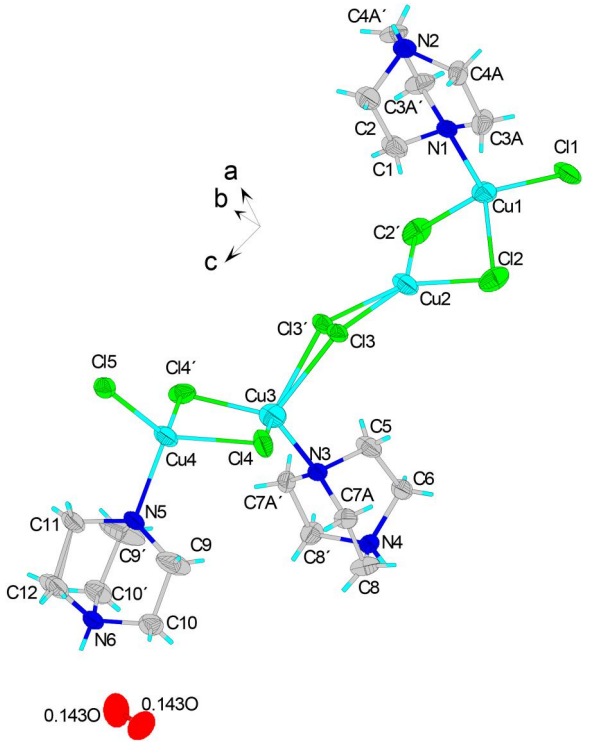

Figure 9. Crystal structure of the compound $(\mathbf{HDABCO^{+}})_3\mathbf{Cu_4Cl_7}$. Protons and atoms with minor occupancies are omitted for clarity.

3. Conclusions

This study considerably extends knowledge about the structural formation of Cu-Cl-DABCO-containing coordination under different synthetic conditions. Compounds **I** and **II** are the result of a 3-component $CuCl_2$-DABCO-HCl composition system study by electrochemical alternating-current synthesis at room temperature. Their appearance covers almost the full diagram, prepared by this method (besides the HCl-rich area). One contains an $HDABCO^{+}$ cation, and the other contains neutral DABCO. They feature 1D inorganic polymeric fragments – $[Cu_2Cl_3^{-}]_n$ and $[CuCl]_n$. Such simplicity of inorganic fragments in this system is caused by soft reaction conditions, which include room temperature, primary alcohols as reaction media (methanol, ethanol), and alternating current on the copper electrodes, promoting the redox comproportionating Cu^{II} and Cu^{0} into Cu^{I}.

Compounds **III**–**VII** are the result of a multivariate character of the $CuCl_2$-DABCO-HCl and CuCl-DABCO-HCl component systems at solvothermal conditions. Variation of starting reagents, solvents, and working temperature has an influence on different chemical processes that are taking place together in the autoclave. Providing higher activation energy and better solubility of insoluble CuCl leads to the formation of different structural geometries, both Cu-Cl inorganic fragments and organometallic derivatives. Using the solvothermal method at 150 °C with ethanol as the solvent, a new MOF compound with copper and DABCO was synthesized. It consists of inorganic

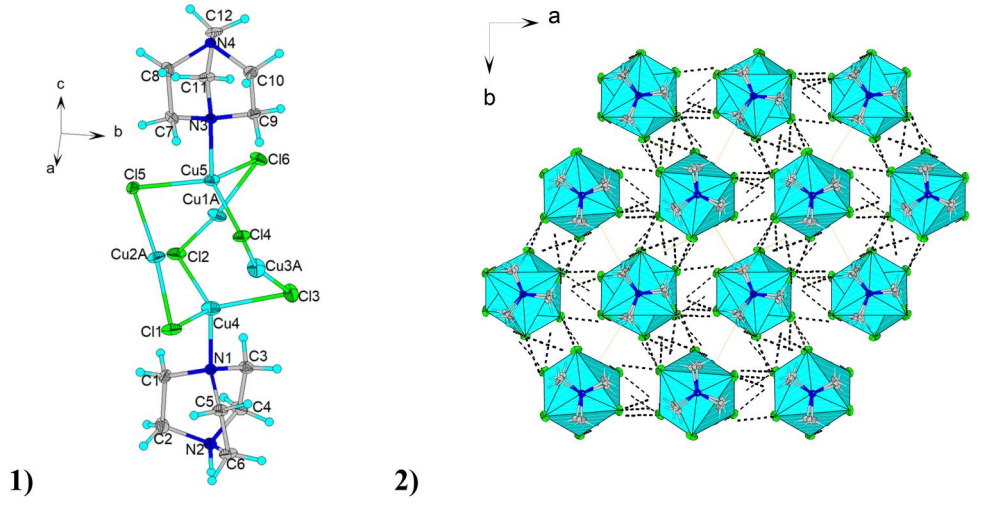

Figure 10. Crystal structure (1) of the compound **($HDABCO^{+}$)Cu_5Cl_6(DABCO)** and molecular chain packing with polyhedral and H-bonds (2). Atoms with minor occupancies are omitted for clarity. H-bonds are dashed.

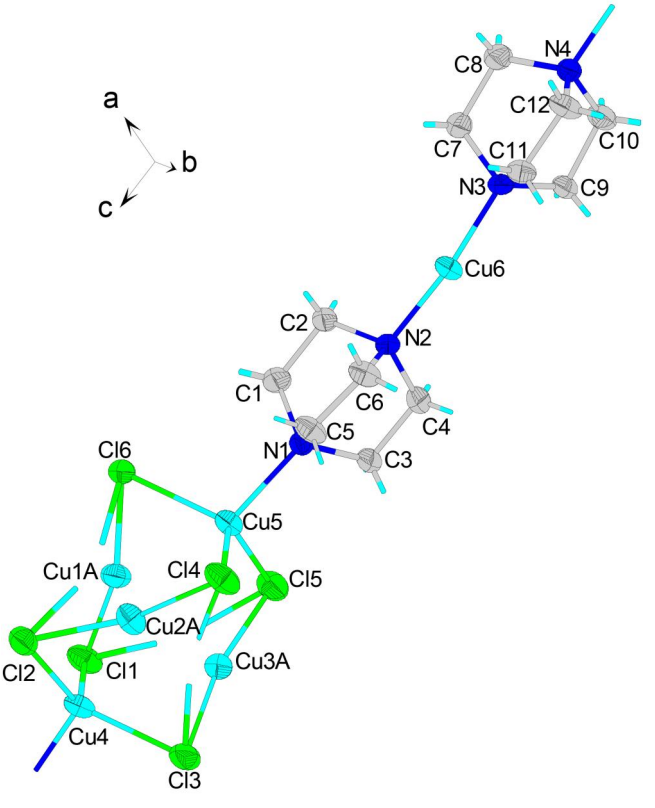

Figure 11. Fragment of an organic–inorganic chain, containing **Cu_5Cl_6** inorganic cluster, two neutral bridging DABCO ligands, and a bridging copper center in the compound **$Cu_6Cl_6(DABCO)_2$**. Protons and atoms with minor occupancies are omitted for clarity.

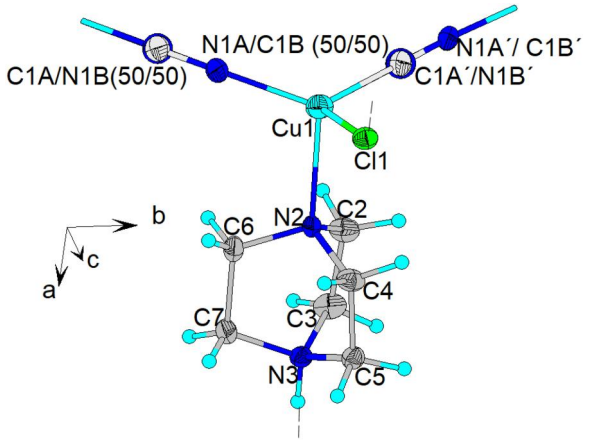

Figure 12. Monoprotonated **HDABCO$^+$** monocation and terminal chloride anion coordinated with cuprocyanide **[Cu(CN)]$_n$** chains the compound **(HDABCO$^+$)CuCl(CN)**.

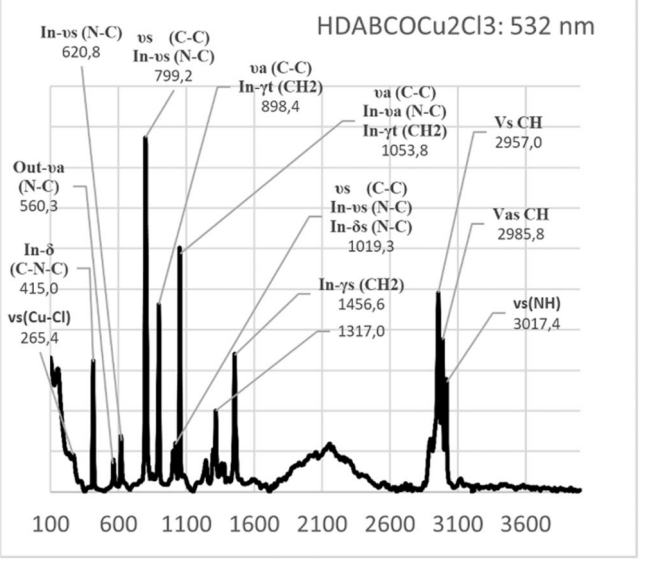

Figure 13. The Raman spectrum of (HDABCO$^+$)Cu_2Cl_3.

$Cu^I_4Cl_6$ clusters connected by DABCO ligands as bridges, forming a 3-D porous framework around $Cu^{II}(H_2O)_4$ fragments. This approach also yielded a compound containing chains of Cu_5Cl_6 clusters, a bridging copper cation, and two bridging DABCO ligands. Increasing the synthetic temperature even by 20 °C (from 130 °C to 150 °C) leads to spatial geometry complication due to achieving the required activation energy for complicated CuCl configurations. It is observed in the case of compounds **III** and **IV**, where the inorganic part of IV, which appeared at 130 °C, is represented as simple elongated Cu_4Cl_7 oligomers, and inorganic Cu_4Cl_6 clusters of complex structural geometry, bridged by neutral DABCO linkers, appeared at 150 °C.

Changing the solvent from ethanol to methanol can shift the region in which certain compounds, such as Cu_2Cl_2(DABCO), appear. It can also result in the formation of

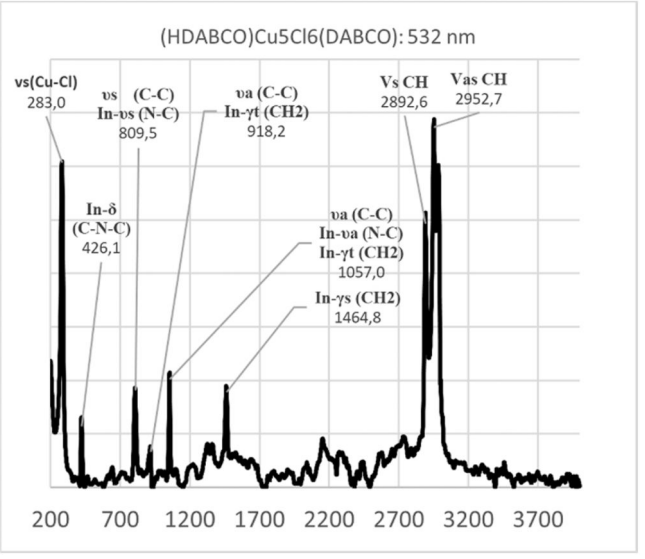

Figure 14. The Raman spectrum of **(HDABCO$^+$)Cu_5Cl_6(DABCO)**.

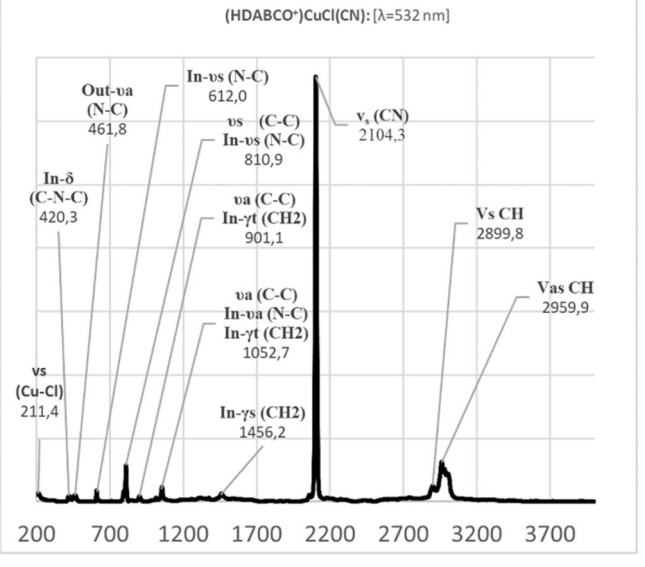

Figure 15. The Raman spectrum of **(HDABCO$^+$)CuCl(CN)**.

entirely different compounds in the same area of the composition space diagram, as seen with the formation of $[Cu(H_2O)_4][Cu_4Cl_6(DABCO)_4]$ and $(HDABCO^+)_3Cu_4Cl_7$ in ethanol, and $(HDABCO^+)Cu_5Cl_6(DABCO)$ in methanol, within the same region of the composition space diagram.

Controlling the acidity of the reaction medium also leads to structural diversity, mostly influenced by the protonation of DABCO amine groups. Diprotonated H_2DABCO^{2+}, which appeared in a high-acidic area with low pH ($\leq$3) of reaction

mixtures, acts as a countercation to anionic CuCl fragments. Monoprotonated $HDABCO^+$, which appeared in the middle-acidic area (pH 4–7), acts as both a countercation and a coordinated ligand to copper. NH fragment often forms H-interactions with neighboring situated acceptor atoms (Cl, N), which leads to bringing inorganic fragments together and orienting them in one direction. Unprotonated DABCO appears in the low-acidic media. Here, a part of the DABCO acts as a soft base for reaction medium, slightly increasing the pH [37]. In such conditions, both amine groups remain open for coordination with each neighboring metal centers. Unprotonated DABCO serves as a bridging ligand, connecting clusters into chains and frameworks (compounds **III** and **VI**) and chains into networks (compound **II**).

Increasing the temperature of the solvothermal method to 170 °C and changing the solvent to acetonitrile results in the formation of a compound that also contains a CN ligand, due to the decomposition of acetonitrile. This *in situ*-formed ligand acts as a bridge and forms infinite 1-D polymeric chains with monovalent copper.

As a result, all the described compounds cover almost the whole CuCl–DABCO–HCl composition space diagram, and we can conclude the completeness of Cu^I-Cl–DABCO-containing compounds in this diagram, prepared by electrochemical and solvothermal methods. In particular, we can use the results of these diagrams for the approximate prediction of the inorganic fragment appearance by repeating the synthetic parameters with other N-containing organic ligands, taking into account some ligand effects on the reaction medium.

Acknowledgments

The authors acknowledge the financial support from the Slovenian Research Agency (research core funding No. P1–0045; Inorganic Chemistry and Technology).

Author contributions

CRediT: **Andrii Hultiaiev**: Investigation, Validation, Visualization, Writing – original draft; **Evgeny Goreshnik**: Conceptualization, Methodology, Project administration, Supervision, Writing – review & editing.

Disclosure statement

The authors declare no conflicts of interest.

Funding

This work was supported by the Slovenian Research Agency ARIS under grant No. P1–0045; Inorganic Chemistry and Technology.

ORCID

Andrii Hultiaiev http://orcid.org/0009-0006-7757-9534
Evgeny Goreshnik http://orcid.org/0000-0002-4675-2190

References

[1] M. Alia, H. Ullah, R. Khan, N.U. Islam, E. Khan, M. Ahmada, A. Ullaha, A. Beguma, G. Ali, Y. Xie. *Royal Soc. of Chem. Adv.*, 16, 2816–2849 (2026).
[2] J.G. Haasnoot. *Coord. Chem. Rev.*, **200-202**, 131–185 (2000).
[3] F. Lacemon, A. Lorbach, A. Eichhorn, F. Cisnetti, A. Steffen. *Chem. Commun.*, 52, 2932–2935, (2015).
[4] C. Santini, M. Pellei, V. Gandin, M. Porchia, F. Tisato, C. Marzano. *Chem. Rev.*, **114**, 815–862 (2014).
[5] M. Gennari, M. Lanfranchi, R. Cammi, M.A. Pellinghelli, L. Marchiò. *Inorg. Chem.*, **46**, 10143–10152 (2007).
[6] E.A. Goreshnik, L.Z. Ciunik, Y. Gorelenko, M.G. Mys'kiv. *Zeitschr. Anorg. allge Chem.*, **630**, 2743–2748 (2004).
[7] A.N. Paesch, A.K. Kreyenschmidt, R. Herbst-Irmer, D. Stalke. *Inorg. Chem.*, **58**, 7000–7009 (2019).
[8] M. Munakata, T. Kuroda-Sowa, M. Maekawa, A. Honda, S. Kitagawa. *J. Chem. Soc, Dalton Trans.*, **19**, 2771 (1994).
[9] A. Vakulka, E.A. Goreshnik. *Jour. of Coord. Chem.*, **71**, 2426–2440 (2018).
[10] D. Rasale, K. Patil, B. Sauter, S. Geigle, S. Zhanybekova, D. Gillingham. *Chem. Commun.*, **54**, 9174–9177 (2018).
[11] E.A. Goreshnik. *Cryst. Eng. Comm.*, **23**, 7171–7178 (2021).
[12] A. Szadkowska, R. Pawłowski, E. Zaorska, S. Staszko, D. Trzybiński, K. Woźniak. *Applied Organom. Chemis.*, **33**, 4983 (2019).
[13] L.R. Collins, J. Lowe, M.F. Mahon, R.C. Poulten, M.K. Whittlesey. *Inorg. Chem.*, **53**, 2699–2707 (2014).
[14] E.R. Williams, M.T. Weller. *CrystEngComm.*, **15**, 31–33 (2013).
[15] M. Eddaoudi, D.F. Sava, J.F. Eubank, K. Adil, V. Guillerm. *Chem. Soc. Rev.*, **44**, 228–249 (2015).
[16] N.S. Rannulu, M.T. Rodgers. *Phys. Chem. Chem. Phys.*, **7**, 1014–1025 (2005).
[17] K. Adil, M. Leblanc, V. Maisonneuve. *J. Fluor. Chem.*, **127**, 1349–1354 (2006).
[18] E.A. Goreshnik. *J. Coord. Chem.*, **70**, 859–870 (2017).
[19] M. Wei, R.D. Willett. *Inorg. Chem.*, **35**, 6381–6385 (1996).
[20] C.R. Groom, I.J. Bruno, M. Lightfoot, S.C. Ward. *Acta Crystallogr. B Struct. Sci. Cryst. Eng. Mater.*, **72**, 171–179 (2016).
[21] R. Seetharaj, V. Vandana, Arya, S. Mathew. *Arab. J. Chem.*, **12**, 295–315 (2016).
[22] C. Dey, T. Kundu, B. Biswal, A. Mallick, R. Banerjee. *Acta Crystallogr. Sect. B*, **70**, 3–10 (2014).
[23] D.-A. Yang, H.-Y. Cho, J. Kim, S.-T. Yang, W.-S. Ahn. *Energy Environ. Sci.*, **5**, 6465–6473 (2012).
[24] X. Wu, Z. Bao, B. Yuan, J. Wang, Y. Sun, H. Luo, S. Deng. *Micropor. Mesopor. Mater.*, **180**, 114–122 (2013).
[25] Y.W. Chen, D.F. Lv, J.L. Wu, J. Xiao, H.X. Xi, Q.B. Xia, Z. Li. *Chem. Eng. J.*, **308**, 1065–1072 (2017).
[26] Y.-R. Lee, J. Kim, W.-S. Ahn. *Korean J. Chem. Eng.*, **30**, 1667–1680 (2013).
[27] Z.N. Gafurov, A.O. Kantyukov, A.A. Kagilev, O.G. Sinyashin, D.G. Yakhvarov. *Coord. Chem. Rev.*, **442**, 213986 (2021).
[28] B.A. Frontana-Uribe, R.D. Little, J.G. Ibanez, A. Palma, R. Vasquez-Medrano. *Green Chem.*, **12**, 2099–2119 (2010).
[29] H.J. Schäfer. *Comptes Rendus. Chimie, Green and Sustainable Chemistry*, **14**, 745–765 (2011).
[30] K. Kamal, M.A. Bustam, M. Ismail, D. Grekov, A. Mohd Shariff, P. Pré. *Pré. Materials*, **13**, 2741 (2020).
[31] "CrysAlisPro, Version 1.171.37.31," Agilent Technologies, [Online]. Available: CrysAlis171.NET. [Accessed 14 01 (2014

[32] G.M. Sheldrick. *Acta Crystallogr. A Found Adv.*, **71**, 3–8 (2015).
[33] O.V. Dolomanov, L.J. Bourhis, R.J. Gildea, J.A.K. Howard, H. Puschmann. *J. Appl. Crystallogr.*, **42**, 339–341 (2009).
[34] A.L. Spek. *Acta Crystallogr. D Biol. Crystallogr.*, **65**, 148–155 (2009).
[35] Dr. K. Brandenburg. GbR DrHP, [Online]. Available: http://www.crystalimpact.com/diamond.
[36] Y.-Y. Liu, M. Grzywa, M. Weil, D. Volkmer. *J. Sol. State Chem.*, **183**, 208–217 (2010).
[37] D.A. Guzonas, D.E. Irish. *Can. J. Chem.*, **66**, 1249–1257 (1988).
[38] A. Burg, D. Meyerstein. *Adv. Inorg. Chem.*, **64**, 219–261 (2012).
[39] W. Liu, W. Lustig, J. Li. *Energy Chem.*, **1**, 2, 100008 (2019).